**Atmospheric
Chemistry
and Physics**

Balloon-borne stratospheric BrO measurements: comparison with Envisat/SCIAMACHY BrO limb profiles

M. Dorf[1], **H. Bösch**[1,*], **A. Butz**[1], **C. Camy-Peyret**[2], **M. P. Chipperfield**[3], **A. Engel**[4], **F. Goutail**[5], **K. Grunow**[6], **F. Hendrick**[7], **S. Hrechanyy**[8], **B. Naujokat**[6], **J.-P. Pommereau**[5], **M. Van Roozendael**[7], **C. Sioris**[9], **F. Stroh**[8], **F. Weidner**[1], **and K. Pfeilsticker**[1]

[1]Institut für Umweltphysik, University of Heidelberg, Heidelberg, Germany
[2]Laboratoire de Physique Moléculaire pour l'Atmosphère et l'Astrophysique (LPMAA), Université Pierre et Marie Curie, Paris, France
[3]Institute for Atmospheric Science, School of Earth and Environment, University of Leeds, Leeds, UK
[4]Institute for Atmosphere and Environment, J. W. Goethe University Frankfurt, Frankfurt, Germany
[5]Service d'Aeronomie du CNRS, Verrières le Buisson, France
[6]Meteorologisches Institut, Freie Universität Berlin, Berlin, Germany
[7]Belgian Institute for Space Aeronomy (BIRA-IASB), Brussels, Belgium
[8]Forschungszentrum Jülich GmbH, Institut für Chemie und Dynamik der Geosphäre ICG-I: Stratosphäre, Jülich, Germany
[9]Harvard-Smithsonian Center for Astrophysics, Cambridge, USA
[*]now at: Jet Propulsion Laboratory (JPL), Pasadena, USA

Abstract. For the first time, results of four stratospheric BrO profiling instruments, are presented and compared with reference to the SLIMCAT 3-dimensional chemical transport model (3-D CTM). Model calculations are used to infer a BrO profile validation set, measured by 3 different balloon sensors, for the new Envisat/SCIAMACHY (ENVIronment SATellite/SCanning Imaging Absorption spectroMeter for Atmospheric CHartographY) satellite instrument. The balloon observations include (a) balloon-borne in situ resonance fluorescence detection of BrO (Triple), (b) balloon-borne solar occultation DOAS measurements (Differential Optical Absorption Spectroscopy) of BrO in the UV, and (c) BrO profiling from the solar occultation SAOZ (Systeme d'Analyse par Observation Zenithale) balloon instrument. Since stratospheric BrO is subject to considerable diurnal variation and none of the measurements are performed close enough in time and space for a direct comparison, all balloon observations are considered with reference to outputs from the 3-D CTM. The referencing is performed by forward and backward air mass trajectory calculations to match the balloon with the satellite observations. The diurnal variation of BrO is considered by 1-D photochemical model calculation along the trajectories. The 1-D photochemical model is initialised with output data of the 3-D model with additional constraints on the vertical transport, the total amount and photochemistry of stratospheric bromine as given by the various balloon observations. Total $[Br_y]=(20.1\pm2.5)$ pptv obtained from DOAS BrO observations at mid-latitudes in 2003, serves as an upper limit of the comparison. Most of the balloon observations agree with the photochemical model predictions within their given error estimates. First retrieval exercises of BrO limb profiling from the SCIAMACHY satellite instrument on average agree to around 20% with the photochemically-corrected balloon observations of the remote sensing instruments (SAOZ and DOAS). An exception is the in situ Triple profile, in which the balloon and satellite data mostly does not agree within the given errors. In general, the satellite measurements show systematically higher values below 25 km than the balloon data and a change in profile shape above about 25 km.

1 Introduction

Inorganic bromine ($Br_y=Br+BrO+BrONO_2+BrOH+BrCl+HBr$) is the second most important halogen affecting stratospheric ozone (WMO, 2003). Although much less abundant than chlorine (see below), stratospheric bromine currently contributes about 25% to global ozone loss due to its much larger ozone depletion efficiency (factor of 45)

Correspondence to: M. Dorf
(marcel.dorf@iup.uni-heidelberg.de)

compared to chlorine. Recent measurements of CH_3Br and man-made halons in the air, sampled at ten remote sites across the globe, suggest that the bromine tied to these organic bromine precursors peaked at about 17 pptv (parts per trillion by volume) around 1998 and since then has declined by 5%/year (Montzka et al., 2003). In 5.6 year old stratospheric air, which was probed in early 1999, the total amount of organic bromine compounds was measured at 18.4 $(+1.8/-1.5)$ pptv and inorganic Br_y was inferred at 21.5 ± 3 pptv (Pfeilsticker et al., 2000). This estimate of total stratospheric bromine indicates possible contributions to stratospheric Br_y from short-lived halogens such as $CHBr_3$ and CH_2BrCl or due to transport of bromine bearing inorganic gases (BrO, HBr, HOBr, ...) or bromine containing aerosols across the tropopause (WMO, 2003; Murphy et al., 1997; Salawitch et al., 2005). Furthermore, accounting for time lags due to transport from the troposphere into the stratosphere and for photochemical destruction of the organic precursor molecules, the surface bromo-organic measurements suggest that stratospheric bromine is likely to have peaked around 2001 with Br_y close to 20–21 pptv (WMO, 2003; Montzka et al., 2003; Dorf et al., unpublished results).

During daylight the most abundant stratospheric bromine species is BrO, which accounts for 60−70% of total Br_y (Lary, 1996; Lary et al., 1996). Fortunately BrO is also the most feasible inorganic bromine species for detection. Detection of atmospheric BrO in the past relied on (1) resonance fluorescence of Br atoms formed by reaction with excess NO added to the probed air (Brune et al., 1989), or (2) UV/visible spectroscopy of either (2a) scattered skylight analysed from the ground, (2b) direct sunlight observed from balloon payloads and (2c) backscattered sunlight detected from space (e.g. Fish et al., 1995; Harder et al., 1998; Wagner and Platt, 1998; Van Roozendael et al., 2002; Pundt et al., 2002). Since balloon-borne BrO profiling is by nature infrequent with respect to both spatial and temporal coverage, improved instrumentation was required to monitor atmospheric BrO more closely. This shortcoming is only partially overcome by atmospheric BrO observations performed by the Global Ozone Monitoring Experiment (GOME) which has routinely monitored global atmospheric BrO vertical columns since 1996.

The SCIAMACHY instrument on the European Envisat satellite provides the possibility of profiling BrO from space and receiving a global coverage within 3 days. Envisat was launched into a sun-synchronous low earth orbit on 28 February 2002. SCIAMACHY is a UV/visible/near-IR spectrometer, covering the wavelength range from 220 nm to 2380 nm at a moderate resolution of 0.2 nm–1.5 nm (FWHM). It measures either direct sunlight during solar occultation, sunlight scattered by the moon during lunar occultation or sunlight scattered by the Earth's atmosphere in nadir or limb direction (e.g. Bovensmann, 1999). In limb scattering mode, SCIA-MACHY scans the Earth's atmosphere vertically in steps of 3.3 km from the ground to about 100 km tangent height with a vertical field of view (FOV) at the tangent point of ~2.8 km

and a horizontal FOV of ~110 km. A horizontal scan is performed at each tangent height covering 960 km.

In order to exploit their full capacity, new satellite observations as performed by SCIAMACHY need to be validated by means of other established methods. In the case of atmospheric BrO limb profiling, validation is quite a challenging task not only because atmospheric BrO concentrations are low ($<2\times10^7$ molecules/cm^3) implying rather low atmospheric BrO absorption in the UV (Optical Densities < several 10^{-3}), but also because BrO is subject to considerable diurnal variation. Validation thus requires either perfect collocation of the validation observation with the satellite profiling (which in practice is not possible, see below), or other methods to account properly for possible temporal or spatial mismatches between sets of observations.

This paper reports on balloon-borne BrO profile measurements using different techniques, performed within the scope of Envisat/SCIAMACHY validation, which were performed for a wide range of geophysical conditions (high, mid and low latitudes during different seasons). For validation purposes these measurements were coordinated to occur close to Envisat/SCIAMACHY overpasses. However, the large diurnal variation of the BrO radical, the different measurement geometries, the duration of the different profile observations and, to a lesser extent, presumably small spatial gradients in total stratospheric bromine (and thus BrO) prevent a direct comparison of the balloon-borne and satellite limb measurements.

Moreover, since the different instruments for BrO validation cannot be employed simultaneously and have different sources of random and systematic errors, a direct comparison of these established techniques is virtually impossible.

To overcome these difficulties, this study uses the following approach: All balloon-borne BrO observations are considered with reference to simulations of the 3-D CTM (Chemical Transport Model) SLIMCAT (Chipperfield, 1999; Chipperfield et al., 2005). If available, the referencing is achieved by comparing the model data with measured dynamic parameters (such as source gas profiles of N_2O, CH_4, ...) and photochemical parameters (profiles of O_3, NO_2, ...). In a second step, matching forward and backward air mass trajectories between the balloon and satellite observations are calculated (e.g. Lumpe et al., 2002; Reimer and Kaupp, 1997; Danilin et al., 2002). A 1-D photochemical model is run along the air mass trajectories on different altitude levels. The 1-D model is initialised with output data of the 3-D model and further constrained by measured dynamic and photochemical parameters. The total stratospheric bromine, obtained by one of the validation instruments (DOAS, see below), is also constrained in the 3-D and 1-D models. Finally, based on the different observations and dynamic and photochemical calculations, stratospheric BrO profiles adequate for comparison with SCIAMACHY are calculated. For some test cases first retrievals of SCIAMACHY BrO profiles are compared with these validation profiles.

The paper is organised as follows; Sect. 2 briefly describes the techniques, methods and tools used to obtain the BrO profiles from the individual instruments and to model the photochemical change along trajectories. Section 3 reports on the individual measurements and comparisons with the SCIA-MACHY BrO observations. Section 4 is mostly devoted to describing further constraints of the 3-D model predictions as given by the various observations. These findings are interpreted and discussed in Sect. 5 with respect to inherent errors of each measurement technique. Section 6 concludes the study and considers the lessons learned for future investigations using the described methods.

2 Methods

2.1 Balloon-borne BrO measurements

2.1.1 Resonance fluorescence BrO measurements

Stratospheric profiles of BrO were measured in situ using the well-established chemical-conversion resonance fluorescence technique (Brune et al., 1989). Stratospheric air is sucked through a rectangular duct by means of a Roots pump. The duct consists of an air inlet, an NO injector, one chlorine and two bromine detection modules stacked behind each other. NO is periodically injected into the air stream in order to convert BrO molecules to bromine atoms in a fast chemical reaction. The atoms are detected downstream by means of a resonance fluorescence arrangement working at 131.8 nm and consisting of a vacuum UV emission lamp and photomultiplier in a rectangular configuration. The photomultiplier signal consists of a background signal, due to Rayleigh and chamber scatter, and the Br resonance fluorescence signal when NO is added. From the difference signal between NO on and off periods (10 s each) Br atom concentrations can be derived employing a pressure dependent calibration. Laboratory calibrations are carried out before and after each flight using the fast chemical titration of chlorine atoms by molecular bromine to ensure the accuracy of the measurements (Brune et al., 1989; Toohey et al., 1990). In brief, a known amount of chlorine atoms is titrated by bromine molecules forming an equivalent amount of bromine atoms and BrCl molecules in a very fast and quantitative reaction. The chlorine atom concentration is measured by vacuum UV absorption using the absorption cross section as determined by Schwab and Anderson (1987). Measured Br atom concentrations are converted into BrO initial concentrations by means of a kinetic model employing seven relevant reactions generating and consuming Br atoms and measured temperatures and pressures. In this model, reaction rates as recommended by Sander et al. (2003) and rates as determined from intercomparisons of the independent Br atom measurements in modules B and C are used. Details are subject to a forthcoming publication. The overall accuracy of the measurements generally is about 35% for BrO with a detection limit of about 5 pptv within 1 min integration time in the altitude range between 18 and 30 km. Lower down, measurements suffer from oxygen absorption and at low pressures, starting at around 30 km, wall loss of Br atoms in the flow tube noticeably effects the measurement, explaining a possible low bias.

Within the framework of the SCIAMACHY validation campaigns, the TRIPLE multi-instrument payload performed 3 validation flights. TRIPLE consists of the Jülich ClO/BrO in situ instrument described above, the cryogenic whole air sampler of the University of Frankfurt for observation of long-lived tracers and the Jülich Fast in situ Stratospheric Hygrometer (FISH). An ECC ozone sonde (electrochemical concentration cell) was onboard for all flights, except on 9 June 2003.

2.1.2 DOAS BrO measurements

Since 1996 stratospheric BrO has been measured by balloon-borne solar occultation DOAS (e.g. Platt, 1994; Ferlemann et al., 2000; Harder et al., 1998). Solar occultation spectroscopy involves the measurement of the line-of-sight UV absorption (called BrO-SCD) of atmospheric BrO (typical optical densities are $10^{-4}-10^{-3}$ for UV vibration absorption bands). The direct solar spectra are collected onboard the azimuth-controlled LPMA/DOAS (Limb Profile Monitor of the Atmosphere/Differential Optical Absorption Spectroscopy) balloon payload. The LPMA/DOAS payload carries a sun-tracker (Hawat et al., 1995) and three optical spectrometers (two grating and one FT-spectrometer; e.g. Camy-Peyret et al., 1993) which analyse direct sunlight over virtually the entire wavelength band ranging from the UV into the mid-IR.

In addition to the spectrometers observing direct sunlight, a small, versatile UV/visible spectrometer has been operated in limb geometry observing scattered sunlight onboard the balloon gondola since 2002. The instrumental setup, performance and first results are published in Weidner et al. (2005). The inferred O_3, NO_2 and BrO abundances correspond well with the data inferred from direct sun measurements.

The BrO evaluation is performed in the wavelength range from 346 nm to 360 nm as recommended by Aliwell et al. (2002). This wavelength range contains the UV vibration absorption bands (4−0 at 354.7 nm, and 5−0 at 348.8 nm) of the $A(^2\pi) \leftarrow X(^2\pi)$ electronic transition of BrO. The set of reference spectra used contains a NO_2 reference spectrum for T=207 K. Two O_3 spectra at T=197 K and T=253 K are fitted to account for temperature effects. The NO_2 and O_3 spectra are recorded with the balloon spectrograph in the laboratory. The NO_2 spectra are calibrated with respect to wavelength and absolute value with the NO_2 cross sections given by Voigt et al. (2002). For this purpose the high-resolution cross section of Voigt et al. (2002) is convolved

to the instrumental resolution of the balloon instrument. The relative wavelength alignment and calibration of the O_3 reference spectra are performed in the same manner with convolved high-resolution cross sections of Voigt et al. (2001).

For O_4 absorptions, the laboratory spectrum of Hermans (2002)[1] is used. The BrO reference is the absolute cross section measured by Wahner et al. (1988), with a spectral resolution of 0.4 nm. The wavelength calibration is taken from own laboratory measurements.

A second-degree polynomial is used to approximate the broad-band extinction such as Mie and Rayleigh scattering. Additionally an intensity offset – a 1st-degree polynomial – is included in the fit to account for the spectrometer stray light. The spectrum recorded at minimum observed air mass, i.e. at balloon float altitude with minimal SZA, is used as Fraunhofer reference spectrum. The total atmospheric SCD is given by the sum of the SCDs retrieved by the fit (the differential SCD) and the amount of absorber in the Fraunhofer reference spectrum, which is obtained by performing a Langley plot (see Fig. 8 and e.g. Ferlemann et al., 1998).

The precision and accuracy of the technique is $\pm 4\%$ and $\pm 12\%$, respectively, or $\pm 5 \times 10^{12}$ molecules/cm^2 (whichever number is larger) in the inferred BrO-SCDs (Harder et al., 1998, 2000). Profile information on stratospheric BrO was obtained by a least-squares profile inversion technique (Maximum A Posteriori) (Rodgers, 2000). A more detailed description of the DOAS profile inversion can be found in Butz et al. (2005). In general SCD values are not smoothed, except for values recorded between 23.5 and 28.5 km on the LPMA/DOAS balloon flight at Kiruna on 24 March 2004. Strong oscillations of the sun-tracker made it necessary to smooth SCD values with a Gaussian filter of 1.5 km width. For similar reasons a Gaussian filter of 1.0 km width was used for the LPMA/DOAS balloon flight at Aire sur l'Adour on 7 October 2003. Since the altitude grid for profile inversion is 2 km, the results are not expected to be influenced much.

To better estimate the error propagation in the BrO profile, inversion is performed twice. First the BrO SCDs are inverted with the errors as given by the fitting routine. Since the error of the fitting routine is not purely statistical it already includes systematic errors of the fit resulting, for example, from the misalignment of the different absorption cross sections (Ferlemann et al., 1998). A second inversion is performed with a systematic offset error added to the BrO SCDs. This error is estimated by Gaussian error propagation from a 10% SCD error, which accounts for temperature effects and uncertainties of the BrO cross section, and the error of the BrO amount in the Fraunhofer reference spectrum, which is typically $(\pm 0.5$ to $\pm 1.0) \times 10^{13}$ molecules/cm^2. The difference between these two profiles is added directly to the error

bars obtained in the first inversion. Therefore a conservative estimate of profile errors is obtained.

2.1.3 SAOZ BrO measurements

BrO is measured by solar occultation in the $320-400$ nm UV spectral range during the afternoon ascent of the balloon at SZA$<90°$ and at the beginning of sunset from float altitude up to $92°-93°$ SZA, when the contribution of scattered light becomes too large for continuing the measurements. In the following only the ascent data is used. The sunlight is collected by a combination of a conical mirror and diffusers within a field of view of 360° azimuth and $+15°$ to $-5°$ elevation. The spectral resolution of the spectrometer is 0.9 nm with an oversampling of 10. There is no temperature stabilisation. The system is run at ambient temperature, cooling by about 15°C during the flight. The measurements are repeated every 30 s resulting in a vertical sampling of about 200 m during the balloon ascent. A full description of the instrument and the retrieval algorithm can be found in Pundt et al. (2002). The spectral retrieval of BrO slant column densities is carried out with the WINDOAS algorithm (Van Roozendael and Fayt, 2000) according to the settings described in Pundt et al. (2002). Because of the small BrO SCD at relatively high sun during ascent, the data is smoothed with a triangular filter to increase the S/N ratio. As a result, the altitude resolution is degraded to 3 km. Associated random errors are those provided by the spectral fit, averaged within the 3 km layer and divided by the square root of the number of data points. The data recorded in presence of clouds is removed using a colour index method.

Profile retrievals are carried out using the onion peeling technique. Random errors are propagated in the retrieval algorithm. Their amplitude increases at decreasing SZA. The impact of photochemical changes during the balloon ascent, and the contribution of scattered light, are ignored. As shown by Pundt et al. (2002) this may result in a maximum error of 0.17 pptv and 0.3 to 0.4 pptv, respectively. The major systematic error comes from the uncertain estimation of the residual BrO column above float altitude. A constant BrO mixing ratio of 14 ± 2 pptv is generally assumed. The uncertainty arising from this decreases at decreasing altitude and is taken into account in the error bars shown. Systematic errors due to the BrO cross-section's uncertainty and its temperature dependence, estimated at $+5/-10\%$ by Pundt et al. (2002), are not included.

2.2 SCIAMACHY BrO profile retrieval

2.2.1 The Harvard Smithsonian retrieval

The Harvard Smithsonian algorithm is described elsewhere (Sioris et al., 2006). The general spectral fitting and inversion equation are presented in Sioris et al. (2003). Thus the method is only summarized here. Limb scan measurements

---

[1]C. Hermans: private communication, for details see: http://www.oma.be/BIRA-IASB/Scientific/Data/CrossSections/ CrossSections.html, 2002.

contain two independent dimensions, namely wavelength and tangent height (TH). Therefore, the retrieval problem is divided into two steps: the spectral fitting and the inversion to obtain the vertical distribution. Radiances in the lower stratosphere are normalised with radiances from the upper atmosphere. This removes the Fraunhofer and Ring effect structure quite effectively. Absorption cross-sections and other pseudo-absorbers (Sioris et al., 2006) are fitted as basis functions to the normalised radiances, resulting in observed BrO-SCDs, which are then interpolated onto a standard TH grid. This data analysis procedure is mimicked to obtain modelled BrO-SCDs. The modelling involves radiative transfer (RT) simulations (McLinden et al., 2002) to generate radiances that are then spectrally fitted. The vertical profile of BrO in the RT model is updated iteratively until convergence between modelled and measured BrO-SCDs is reached (Sioris et al., 2006). A further convergence criterion has been added: if the agreement between modelled and observed BrO-SCDs at the bottom of the simulated TH range is not within 1%, this relative difference must not increase monotonically with decreasing TH. This protects the retrieval from finding extreme values at the lower altitude limit. On 25 March 2004, the O_3 profile measured by DOAS in ascent (Butz et al., 2005) was used as a forward model input to the SCIAMACHY BrO retrieval since the model (McLinden et al., 2002) O_3 profile deviated from the true condition substantially due to dynamic reasons.

2.3 Modelling

2.3.1 Trajectory modelling

Balloon-borne measurements are inherently restricted by different constraints, limiting their flexibility in satellite validation. First, the launch window depends not only on the surface weather conditions, but also on stratospheric winds which determine the balloon's trajectory and the match location. Furthermore, the probed air masses of some balloon payloads are influenced directly by astronomical parameters, such as the solar zenith angle for solar occultation measurements (e.g., LPMA/DOAS payload). In practice, all these constraints make it difficult to match the temporal and spatial factors of the balloon measurements directly with the individual satellite measurements. Air mass trajectory matching can partly compensate for these restrictions (Lumpe et al., 2002).

Here, air mass trajectory calculations are used for matching the balloon-borne measurements with SCIAMACHY observations. The trajectory model uses the operational analysis and forecasts of the European Centre for Medium Range Weather Forecasts (ECMWF) – or a combination of both – given every 6 h on a 2.5°×2.5° latitude/longitude grid. The ECMWF data is interpolated to 25 user-defined isentropic levels extending from the surface up to 1600 K. The internal time step for integrating the air masses' path is 10 min

and the diabatic and climatological heating rates are based on Newtonian cooling. The results (trajectory points) are stored for each hour (Reimer and Kaupp, 1997; Langematz et al., 1987).

Backward and forward trajectories are started at the balloon measurement locations which depend on the individual measurement technique. In the case of the TRIPLE in situ payload, the air mass trajectory end and start points are given by the balloon trajectory. For the LPMA/DOAS and the SAOZ remote-sensing payloads, the start and end points are calculated from knowledge of the balloon flight trajectory and the known observation geometry given by the line-of-sight for each measurement. For post-flight analysis, air mass forward and backward trajectories are calculated for up to 10 days, but for balloon flight planning purposes the time range is limited by the available ECMWF forecasts (analyses are available up to 12:00 UT of the day before, forecasts for every 6 h up to 72 h).

The actual geolocations of SCIAMACHY observations are taken from the SCIAMACHY Operational Support Team (SOST) on its website (http://atmos.af.op.dlr.de/projects/scops/). Here, the overpass time, the geolocation and detailed measurement specifications (e.g. swath, measurement duration, ground pixel size) can be downloaded for the SCIAMACHY limb and for the SCIAMACHY nadir mode for each Envisat orbit. For the air mass trajectory-based matching technique only the area covered by tangent points (light blue areas in Fig. 1) of SCIAMACHY limb observation is considered in more detail. This information is used to find satellite measurement points along individual air mass trajectories, for which the spatial and temporal mismatch is as small as possible. The match criterion is chosen based on the experience of the ozone Match experiment (von der Gathen et al., 1995): a time mismatch between the satellite observation and the air mass trajectory started at the balloon observation of $<\pm1$ h and an area mismatch of $<\pm500$ km. If SCIAMACHY observations do not fulfil these criteria, the distance criterion is extended up to 1000 km. In this study only SCIAMACHY limb measurements are considered.

2.3.2 Photochemical modelling

As outlined above, the use of a validated 3-D CTM photochemical model is necessary when different measurements of stratospheric radicals are compared and validated. Figure 2 demonstrates why the model has to be used to compare SCIAMACHY BrO limb measurements, left panel, with LPMA/DOAS balloon ascent and occultation observations shown in the right panel. The measured line-of-sight BrO absorption is indicated by the thin black lines in both panels. In addition, the thick black line in the right panel represents the balloon trajectory. Here, the observations are superimposed a photochemical simulation of stratospheric BrO from the SLIMCAT 3-D CTM (Chipperfield, 1999) for 23 March 2003. The observation geometry for SAOZ measurements is
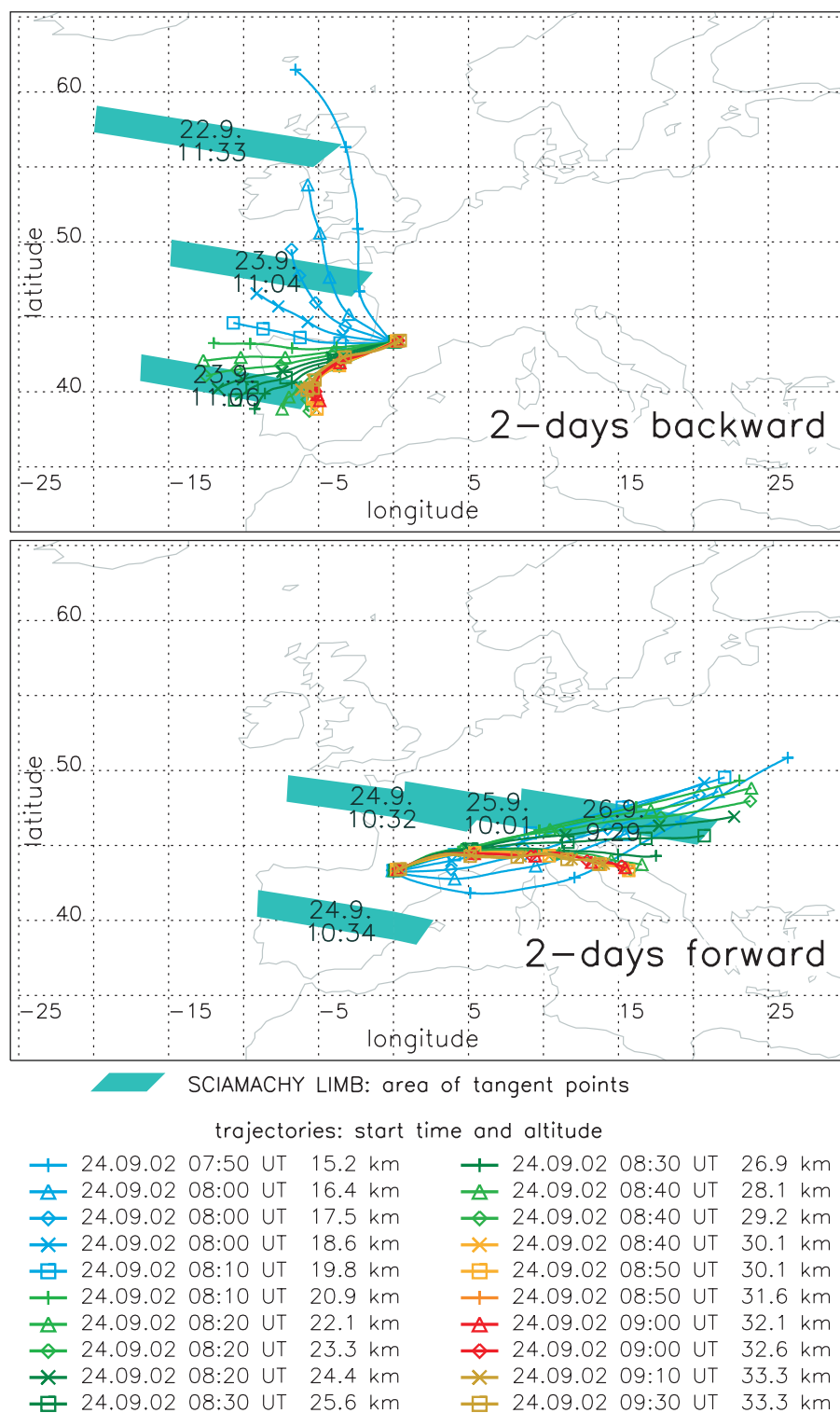
Fig. 1. Two days backward (upper panel) and forward (lower panel) air mass trajectories for TRIPLE ascent observations at Aire sur l'Adour, France, on 24 September 2002. Envisat/SCIAMACHY orbit numbers matching with the TRIPLE trajectory are 2940, 2954, 2968, 2982, 2995, and 2996. The light blue rectangles represent the area probed by SCIAMACHY limb observations.
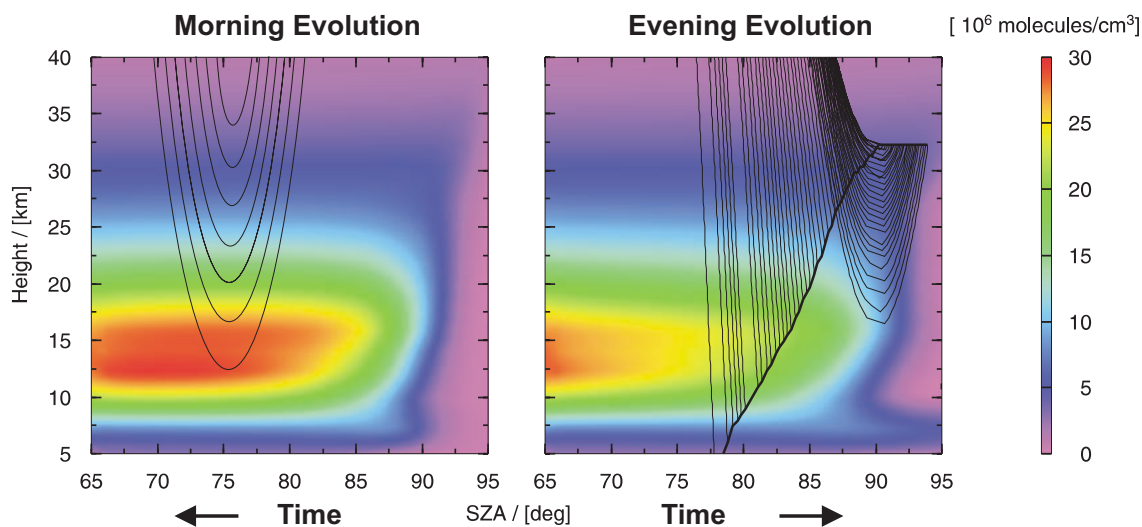
Fig. 2. Colour-coded model concentration field of BrO as a function of height and SZA, for the DOAS balloon flight on 23 March 2003 at Kiruna (67.9° N, 22.1° E). Left and right panels show the morning and evening evolution of BrO, respectively. The black lines in the left panel represent the line-of-sight of a SCIAMACHY limb scan. In the right panel the observation geometry of the DOAS measurements is shown for every twentieth spectrum measured during ascent and every tenth spectrum during solar occultation. The thick black line represents the trajectory of the balloon and the thin black lines indicate the optical path from the Sun to the balloon instrument for measurements during ascent and solar occultation. Note that in the real atmosphere the lines-of-sight are close to being straight lines, but the projection of the Earth's curvature on a straight x-axis causes the lines-of-sight to appear curved in the presentation.

basically the same as for LPMA/DOAS. For TRIPLE observations the situation is less complicated since measurements are performed in situ, but still at varying SZA.

SLIMCAT is a 3-D off-line CTM with detailed treatment of the stratospheric photochemistry. The model temperatures and horizontal winds are specified from analyses and the vertical transport in the stratosphere is diagnosed from radiative heating rates. In the stratosphere the model uses an isentropic coordinate extended down to the surface using hybrid sigma-theta levels (M. P. Chipperfield, private communication). The troposphere is assumed to be well-mixed.

The CTM was integrated with a horizontal resolution of $7.5° \times 7.5°$ and 24 levels extending from the surface to about 55 km. The model was forced using ECMWF analyses and the simulation started on 1 January 1977. The model halogen loading was specified from observed tropospheric CH_3Br and halon loadings (WMO, 2003). In addition, an extra 4 pptv bromine was modelled in a tracer to represent bromine-containing very short-lived species (VSLSs) and 1 pptv was assumed to be transported to the stratosphere as Br_y (M. P. Chipperfield, private communication). Accordingly, the total stratospheric bromine loading around 2000 is approximately 21 pptv. Output was saved at 00:00 UT every 2 days, interpolated to the location of the balloon flights. A 1-D column model was then used to reconstruct the diurnal cycle for comparison with the observations.

The vertical 1-D column model calculates the stratospheric photochemistry on 2-day forward and backward air mass trajectories (described in the previous paragraph) with the aim to find best guess profiles for the satellite observations based on the different validation balloon measurements. The stratospheric photochemistry is modelled on 20 potential temperature (Θ) levels between Θ=323 K ($\simeq$9 km) and Θ=1520 K ($\simeq$42 km). The 1-D column model is initialised, at each height level, at 00:00 UT with 3-D CTM SLIMCAT model results at an adjacent 48 hour model time step at the balloon launch site. If output is not available on the day of the balloon flight, a decision is made whether to take output from the day before or the day after the flight by comparing measured O_3, NO_2 and/or tracers such as CH_4 and N_2O with the model and choosing the output that best matches the measurement.

The model is constrained to follow the evolution of the SZA time-line, which is taken from the air mass trajectory calculations. In satellite validation these measures guarantee that the photochemical evolution of the modelled air mass is a good approximation of the true evolution between initialisation of the model, the satellite measurement and balloon-borne observation. For simplicity a single representative SZA time-line is chosen for all Θ levels and the model is run with fixed pressure and temperature for each Θ level taken from the meteorological support data of the balloon flight.

The 1-D chemistry model is an updated version (using JPL-2002 kinetics; Sander et al., 2003) of the model used by Bösch et al. (2003) and includes a comprehensive set of all relevant gas-phase and heterogeneous reactions. Aerosol loadings are taken from Deshler et al. (2003) as recommended by Dufour et al. (2005). Photolysis rates are

Table 1. Compendium of balloon-borne BrO measurements and Envisat/SCIAMACHY overpasses. BA, BD and SO denote balloon ascent, balloon descent and solar occultation, respectively.

Date Time / UT	Location	Geophys. Cond. SZA range	Instrument Observ. Geom.	Satellite coincidence Orbit, Date, Time/UT	Altitude – range/km	Time – delay/h	Spatial – distance/km
12 Aug 2002 18:15–19:10	Kiruna 67.9° N, 21.1° E	high lat. summer SZA: 85°−89°	SAOZ BA	2342, 11 Aug 2002, 18:21 2352, 12 Aug 2002, 09:37	18–30 5–30	−24.8 −9.6	179–494 182–495
24 Sep 2002 07:08–11:39	Aire sur l'Adour 43.7° N, 0.3° W	mid-lat fall SZA: 44°−88°	TRIPLE BA/BD	2954, 23 Sep 2002, 11:06 2968, 24 Sep 2002, 10:32	21–29 16–33	−21.6 −2.5	379–491 449–499
1 Oct 2002 16:35–17:25	Aire sur l'Adour 43.7° N, 0.3° W	mid lat. fall SZA: 79°−88°	SAOZ BA	3068, 1 Oct 2002, 10:13 3082, 2 Oct 2002, 09:42	13–29 13–29	−7.1 +17.0	278–487 265–493
23 Feb 2003 20:42–21:30	Bauru 22.4° S, 49.0° W	subtropics summer SZA: 76°−85°	SAOZ BA	5145, 23 Feb 2003, 12:56 5160, 24 Feb 03, 14:04	16–21 24–28	−8.2 +16.7	403–486 125–462
6 March 2003 06:25–10:49	Kiruna 67.9° N, 21.1° E	high lat. winter SZA: 72°−86°	TRIPLE BA/BD	5288, 5 March 2003, 12:13 5301, 6 March 2003, 10:04	16–28 5–31	−19.6 +3.7	4–481 403–499
16 March 2003 15:19–16:09	Kiruna 67.9° N, 21.1° E	high lat. spring SZA: 84°−89°	SAOZ BA	5418, 14 March 2003, 14:08 5484, 19 March 2003, 04:52	23–29 16–23	−50.0 +61.2	46–473 9–452
23 March 2003 14:47–17:35	Kiruna 67.9° N, 21.1° E	high lat. spring SZA: 79°−95°	LPMA/DOAS BA/SO	5545, 23 March 2003, 11:07 5558, 24 March 2003, 09:01	18–28 19–29	−5.2 +17.4	268–496 10–495
30 March 2003 16:01–16:53	Kiruna 67.9° N, 21.1° E	high lat. spring SZA: 83°−88°	SAOZ BA	5645, 30 March 2003, 10:49 5658, 31 March 2003, 08:37	5–29 5–23	−6.0 +16.8	88–307 47–494
9 June 2003 04:57–9:52	Kiruna 67.9° N, 21.1° E	high lat. summer SZA: 45°−70°	TRIPLE BA / BD	6652, 8 June 2003, 19:01 6661, 9 June 2003, 10:18	5–31 5–34	−11.6 +5.1	19–499 60–494
9 Oct 2003 15:39–17:09	Aire sur l'Adour 43.7° N, 0.3° W	mid-lat fall SZA: 66°−88°	LPMA/DOAS BA	8407, 9 Oct 2003, 09:51 8421, 10 Oct 2003, 09:20	17–31 25–33	−6.5 +17.2	738–988 547–977
31 Jan 2004 20:54–21:46	Bauru 22.4° S, 49.0° W	subtropics summer SZA: 76°−86°	SAOZ BA	10 040, 31 Jan 2004, 12:06 10 055, 1 Feb 2004, 13:15	25–30 15–21	−9.7 +16.1	287–492 33–488
5 Feb 2004 20:25–21:12	Bauru 22.4° S, 49.0° W	subtropics summer SZA: 70°−80°	SAOZ BA	10 112, 5 Feb 2004, 12:51 10 127, 6 Feb 2004, 13:59	5–21 25–29	−8.0 +17.0	229–495 179–479
24 March 2004 13:55–17:35	Kiruna 67.9° N, 21.1° E	high lat. spring SZA: 72°−95°	LPMA/DOAS BA/SO	10 798, 24 March 2004, 10:35 10 811, 25 March 2004, 08:24	12–33 20–26	−5.4 +17.1	371–499 383–494
17 June 2005 18:32–21:07	Teresina 5.1° S, 42.9° W	tropics winter SZA: 61°−94°	LPMA/DOAS BA/SO	17 240, 17 June 2005, 11:53 17 255, 18 June 2005, 13:02	25–30 5–33	−8.1 +18.4	382–491 6–490

interpolated with respect to pressure, temperature, overhead ozone and solar zenith angle (SZA) from a SLIMCAT lookup table where the actinic fluxes are calculated as recommended by Lary and Pyle (1991) and validated for J_{NO_2} by Bösch et al. (2001).

Furthermore, each BrO observation conducted by the remote sensing instruments SCIAMACHY, SAOZ and DOAS is a composite of changing photochemical conditions (due to changing SZA) along the line-of-sight. Arguably gradients in BrO arising from this effect are the smallest for the SCIAMACHY observations since it takes measurements during late morning (around 10:30 LT), i.e. far from sunset or sunrise. Hence a fixed SZA for SCIAMACHY observations is assumed.

Photochemical-weighting factors are calculated to scale balloon observations to the photochemical conditions of the satellite measurements. In the case of DOAS measurements the scaling is performed prior to profile inversion as described by Butz et al. (2005), thus compensating photochemical changes during the ascent measurements of the balloon. For TRIPLE and SAOZ measurements, the ratio of the model profile at the SZA of the satellite measurement and the model profile at the SZA of the balloon measurement is calculated, and used to scale the profiles accordingly.
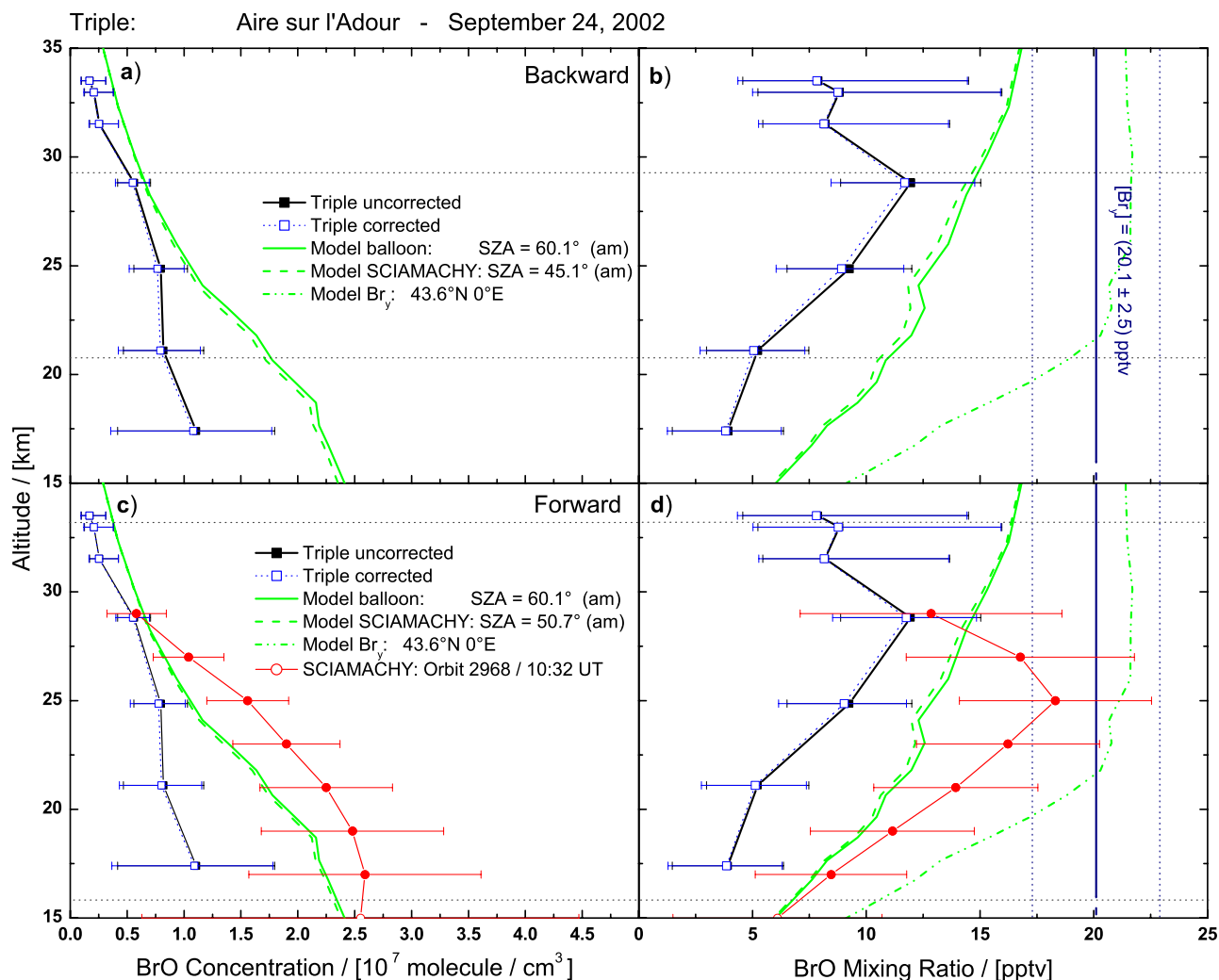
Fig. 3. Comparison of a BrO profile measured by TRIPLE during balloon ascent on 24 September 2002 at Aire sur l'Adour with model calculations and SCIAMACHY limb retrievals. Black squares represent the photochemically-uncorrected balloon measurement and blue squares the balloon profile photochemically corrected to the SZA of the SCIAMACHY measurement. Corresponding model profiles at the SZA of the balloon and satellite observations are shown as solid and dashed green lines respectively. Total inorganic Br_y volume mixing ratios as used in the model (green dash-dotted line) and as retrieved by DOAS measurements (vertical dark blue lines – see text for details) are also indicated. SCIAMACHY measurements are shown as solid red circles in the altitude range for the match (as given in Table 1), which is indicated as thin dotted horizontal lines, and as open red circles ouside this range. Panels **(a)** and **(b)** show calculations for the "best" backward match and panels **(c)** and **(d)** for the "best" forward match. Concentrations and volume mixing ratios are given for each case.

The modelling errors are estimated by sensitivity studies following a similar approach as described in Bracher et al. (2005). Several model runs are performed along a representative air mass trajectory with varying model parameters that are important for the photochemical variation of BrO. These parameters include the NO_2 and O_3 profile ($\pm30\%$), overhead ozone ($\pm35\%$), the temperature for each Θ level (±7 K), the rate constants of reaction $BrO+O_3$ and $BrO+NO_2$ ($\pm20\%$ and $\pm15\%$), the photolysis rate of BrO and $BrONO_2$ ($\pm15\%$) and the aerosol surface area ($\pm100\%$). The root-mean-square deviation of the vertical profiles from the standard run gives the estimate of the modelling error and

therefore the error of the scaling. Although individual profiles can deviate significantly from a standard run profile at the same SZA (e.g. for varied NO_2 profile or J_{BrONO_2} the difference is around 12% and 10% at the concentration maximum, respectively), the scaling of profiles is hardly affected since the ratio of two profiles of the same model run is used. In the relevant altitude layer between 10 km and 30 km a scaling error of 5% was obtained. Whenever photochemically-corrected trace gas profiles are shown, the modelling error is added applying Gaussian error propagation.
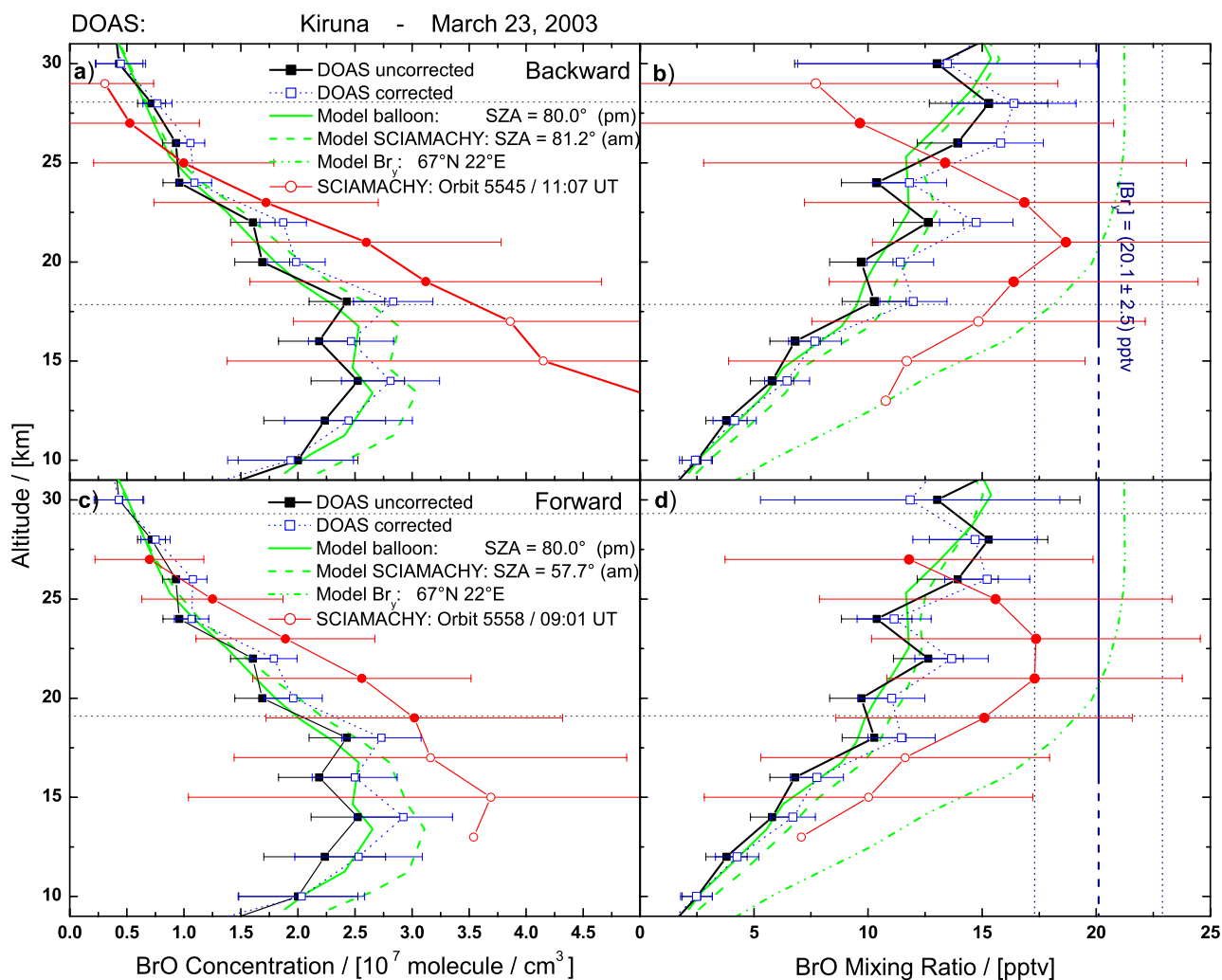
Fig. 4. Same as Fig. 3, but for a BrO profile measured by DOAS during balloon ascent on 23 March 2003 at Kiruna.

3   Observations

An overview of balloon flights conducted within the framework of the SCIAMACHY validation is given in Table 1. It includes information about the date and location of the soundings, the geophysical condition and the SZA range of the measurements (first 4 columns). The right part of the table provides the relevant information with respect to the "best" matching SCIAMACHY limb observations, as indicated by the calculated forward and backward air mass trajectories. For each balloon flight one "best" match is identified for the backward trajectory and one for the forward trajectory calculations. The orbit number and overpass time, the altitude range in which the match obeys the match criteria, the maximum time delay between SCIAMACHY and balloon measurement and the spatial distance between trajectories and SCIAMACHY measurement are given for each match. For future validation exercises using balloon mea-

surements, it is thus recommended to use these identified pixels in SCIAMACHY profile retrieval exercises.

Figures 3 to 7 display the key findings of the study using the examples of a TRIPLE flight conducted on 24 September 2002 at Aire sur l'Adour, France, a SAOZ flight on 31 January 2004 at Bauru, Brazil, and three DOAS flights on 23 March 2003 and 24 March 2004 at Kiruna, Sweden, and on 9 October 2003 at Aire sur l'Adour, France. The examples are chosen in order to cover a wide range of different geophysical conditions. Each figure shows the original measured BrO profiles i.e., the photochemically-uncorrected balloon measurement (solid black squares) and, if available, the matching SCIAMACHY BrO profile (red dots). Both sets of observations show large discrepancies primarily due to (1) inherent errors of the measurements, (2) the different daylight time of the individual observations and thus photochemistry-related changes in stratospheric BrO, or (3) possible spatial gradients in stratospheric bromine, although this factor is less likely.
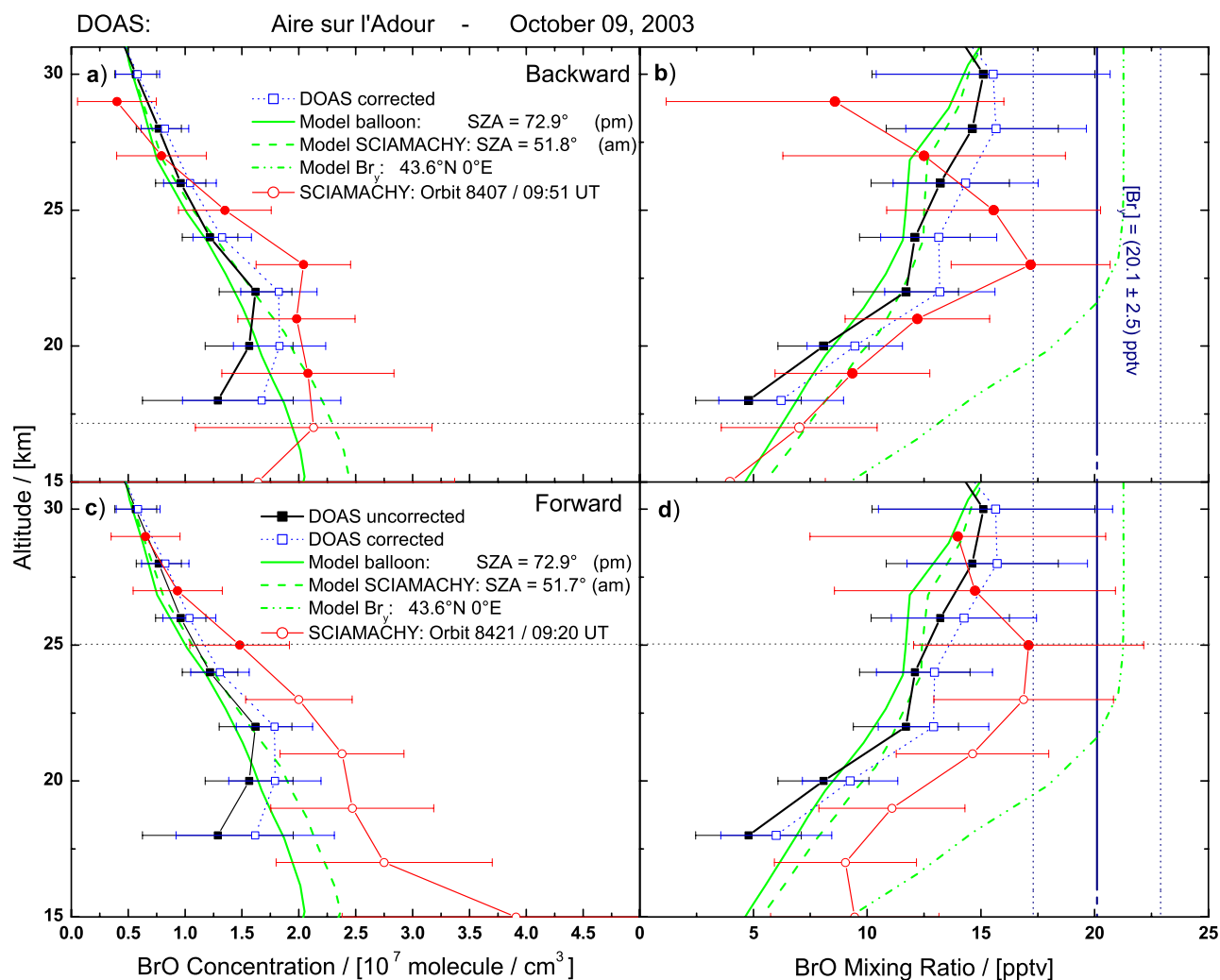
Fig. 5. Same as Fig. 3, but for a BrO profile measured by DOAS during balloon ascent on 9 October 2003 at Aire sur l'Adour.

For reasons related to (1) the reader is recommended to refer to the relevant literature for each of the techniques used (e.g. Pundt et al., 2002; Brune et al., 1989; Ferlemann et al., 1998; Sioris et al., 2006). Within the scope of this study, reasons related to (2) and (3) are dealt with using the trajectory model, the 1-D photochemical model and the SLIMCAT 3-D CTM model. Before correcting the measured BrO profiles for photochemistry and dynamics, further constraints are discussed, which arise from each observation and that can be used for photochemical modelling.

4 Photochemical modelling and its constraints

Before addressing photochemical modelling in more detail, 3 different constraints for the modelling are discussed. These constraints are obtained from the balloon soundings performed within the scope of this study (total stratospheric bromine, vertical transport and photochemical constraints).

Owing to an intensive cross validation of SLIMCAT with field observations – to which the authors have contributed (e.g. Harder et al., 2000) – these constraints have already been partly implemented in SLIMCAT in recent years.

1. **Total stratospheric bromine:** For stratospheric sounding of the LPMA/DOAS payload, total stratospheric bromine (Br_y) can be inferred for altitudes above balloon float altitude. Such a constraint is particularly important because it largely constrains Br_y in the lower stratosphere (taken here from the tropopause to the balloon float altitude). Stratospheric Br_y concentrations are known to have levelled-off in recent years and thus spatial gradients ($\sim$1 pptv across the global stratosphere) in Br_y due to different age of air masses are expected to be small (for details see Montzka et al., 2003). Once total stratospheric Br_y is known, an accurate constraint is available for stratospheric BrO taking $[BrO] \leq [Br_y]$. BrO can in principle be further constrained, though less
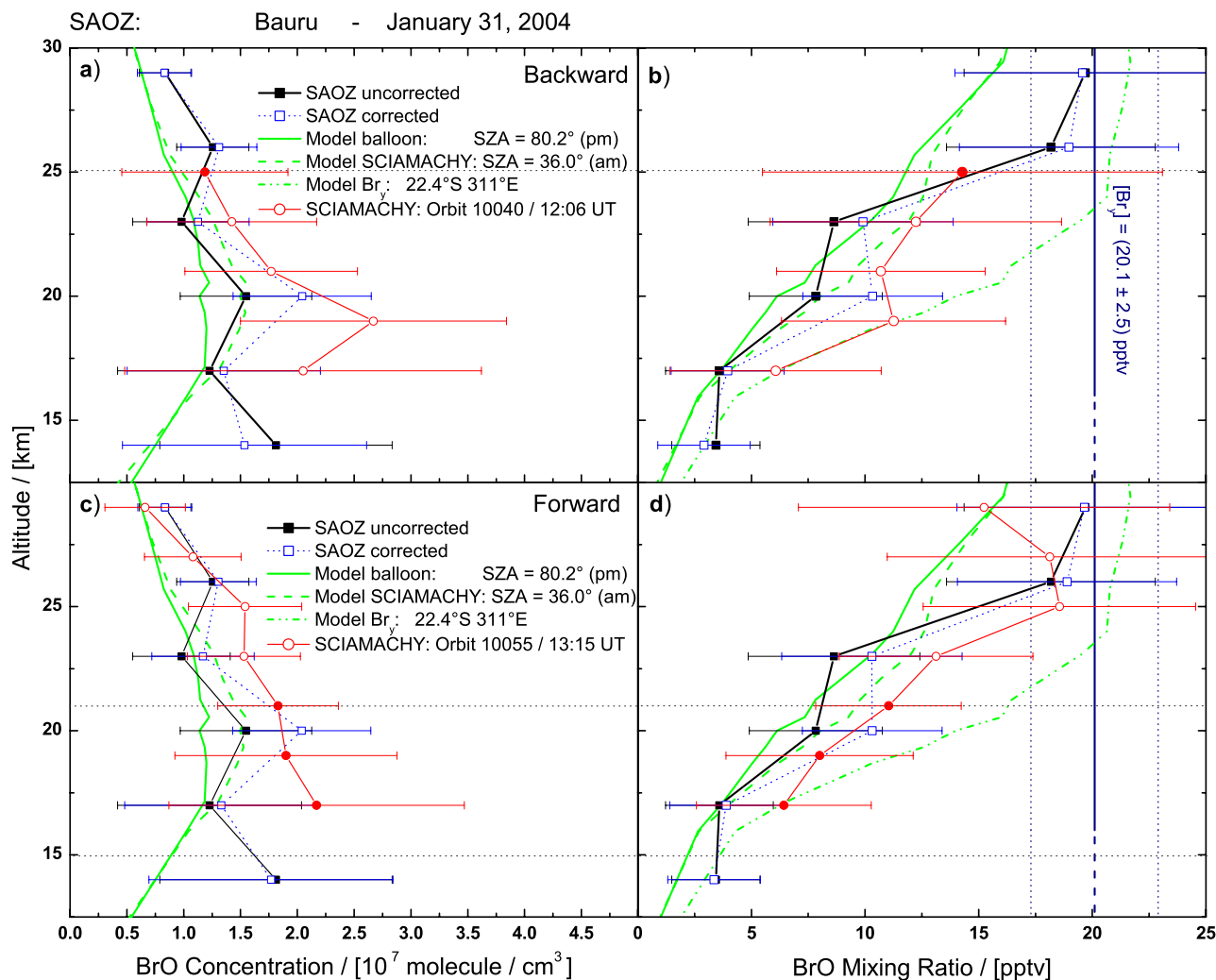
Fig. 6. Same as Fig. 3, but for a BrO profile measured by SAOZ during balloon ascent on 31 January 2004 at Bauru.

accurately, using results from a photochemical model (see below).

Here, observations made on 9 October 2003 at Aire sur l'Adour are presented as an example of how total stratospheric Br_y is inferred from DOAS measurements. A Langley plot is performed, where the slope of measured BrO absorption is analysed as a function of the calculated total air mass at balloon float altitude (33 km), covering a SZA range between 84.27° and 87.52° (Fig. 8). For this observation the slope of the least-squares-fitted data results in an average BrO mixing ratio of (14.5±1.5) pptv above 33 km. The errors of the method are due to uncertainties (a) in the total air mass (±2%) checked by independent temperature and pressure measurements aboard the LPMA/DOAS payload, by two independent ray-tracing codes and by the LPMA CO_2 measurement, (b) the spectral retrieval of BrO (±5%), (c) the absorption cross-section of BrO

(±8%), and (d) the changing [BrO]/[Br_y] ratio above balloon float altitude. This ratio can be obtained by considering the bromine chemistry above balloon float altitude at daytime. In the sunlit upper stratosphere, the most important bromine reactions (≥90%) are

$$BrO + h\nu \longrightarrow Br + O \tag{R1}$$
$$Br + O_3 \longrightarrow BrO + O_2 \quad . \tag{R2}$$

Inaccuracies in this simple photochemical scheme are only due to the BrO cross section, the quantum yield for BrO photo-dissociation (R1), the rate reaction coefficient k_{R2} for Reaction (R2) and the ozone concentration. For this flight, the SLIMCAT calculations show that the [BrO]/[Br_y] ratio is around 0.76 at 33 km, 0.8 at 36 km, 0.76 at 40 km, 0.54 at 45 km, and 0.23 at 50 km. The line-of-sight weighted average is concluded to be 0.72 for these conditions, with
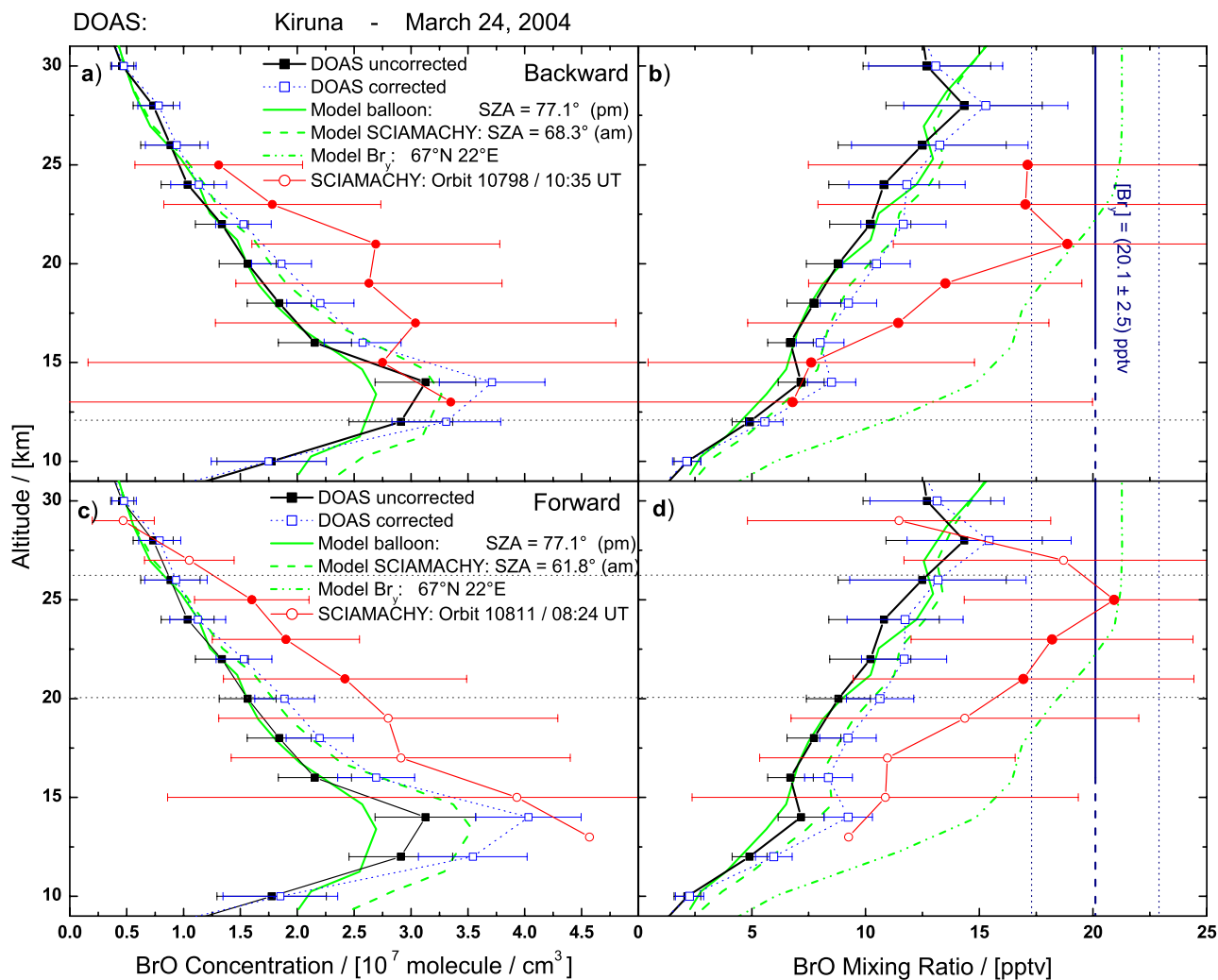
Fig. 7. Same as Fig. 3, but for a BrO profile measured by DOAS during balloon ascent on 24 March 2004 at Kiruna.

the largest uncertainty coming from the uncertainty in k_{R2}, which is ±20% according to Sander et al. (2003). Combining all uncertainties, our measurement indicates [Br_y]=(20.1±2.5) pptv above 33 km at northern mid-latitudes by late 2003. Similar total mixing ratios of Br_y can be obtained from other LPMA/DOAS flights. Putting together all these observations and considering the age of the probed air masses, a trend in stratospheric bromine can be inferred (see Figs. 1–8, WMO, 2003).

2. **Vertical transport:** The diabatic vertical transport in the stratosphere is also known to be of particular concern in 3-D CTM modelling i.e., for high (Arctic) and low (tropical) latitudes (Chipperfield, 1999). In order to compensate for potential deficits in the vertical transport, the tracers N_2O and CH_4, which are available for TRIPLE and LPMA/DOAS flights, are also compared with the 3-D CTM output. Since dynamic tracers are

not measured simultaneously for the SAOZ flights, O_3 is used as an indicator for the vertical transport. In particular, the vertical transport is tested for the balloon flights presented in this study, as follows: For the TRIPLE flight on 24 September 2002 it is found that the measured dynamic tracers N_2O and CH_4 agree excellently with the CTM SLIMCAT simulations. A similar good agreement with SLIMCAT is found for the LPMA/DOAS flight on 23 March 2003. Unfortunately for the 9 October 2003 and the 24 March 2004 LPMA/DOAS flight no LPMA data is available to date, thus measured and modelled tracer profiles cannot be compared. Therefore, the dynamics are verified by the O_3 profile simultaneously recorded with the DOAS instrument. The same procedure was performed for the SAOZ flight on 31 January 2004 since no other transport tracers were available. In all three cases the measured O_3 profile is found to correspond well with the model.
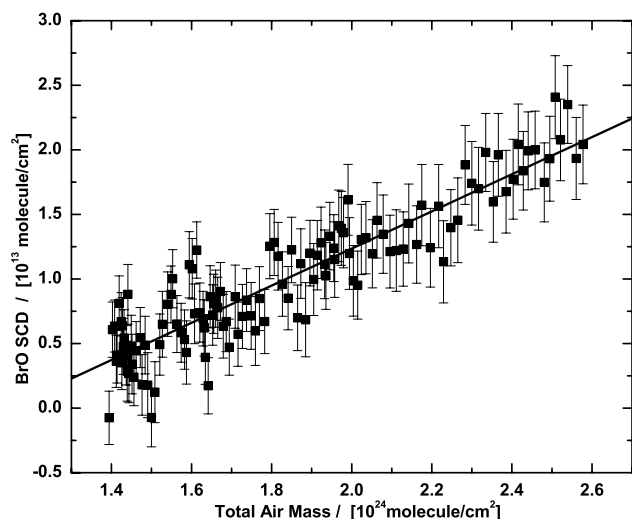
Fig. 8. Measured BrO absorption as a function of the calculated total air mass observed for a SZA range between 84.27° and 87.52° at balloon float altitude (33.5 km) over Aire sur l'Adour on 9 October 2003. The slope of the least-square-fitted data results in the average BrO mixing ratio of (14.4±0.7) pptv above float altitude.

The overall good agreement of the model with the tracer data supports the findings of Feng et al. (2005) who found that the version of SLIMCAT used here, with the CCM radiation scheme, performed well in this respect. Therefore, large uncertainties in the vertical transport are considered unlikely for the balloon flights discussed here.

3. **Photochemistry and its constraints:** Potential disagreement between observations and the model also arises from photochemistry-related uncertainties (e.g. Canty et al., 2005). It is found useful to constrain the 1-D photochemical calculations with the measured abundances of NO_2 and O_3 (Bracher et al., 2005). BrO reacts efficiently with NO_2 to $BrONO_2$, with the photolysis of $BrONO_2$ being the most important back reaction during daytime. Therefore, stratospheric BrO is strongly dependent on NO_2 and an appropriate scaling of the 1-D photochemical modelling may reduce potential errors in BrO comparison studies to a great extent. Fortunately for the SAOZ and DOAS BrO observations such a scaling can easily be performed since NO_2 and BrO profiles are measured simultaneously. For the TRIPLE BrO observation such a scaling of modelled/measured NO_2 is more difficult since the NO_2 is not measured on that payload. Therefore, SCIAMACHY NO_2 observations (Sioris et al., 2004) are used, which were validated by balloon measurements by Butz et al. (2005).

The SCIAMACHY NO_2 profile for the TRIPLE flight on 24 September 2002 matches the model values between 22 and 33 km but shows up to 50% smaller con-

centrations below 22 km. The accuracy of the SCIAMACHY measurements is discussed in Butz et al. (2005). Model values of NO_2 for the SAOZ flight on 31 January 2004 basically agree with the measured profile within the given error bars below 25 km but are systematically lower (~30% at 20 km). Above 25 km, up to balloon float altitude at around 30 km, the agreement is very good. For the DOAS flight on 23 March 2003 the model NO_2 shows systematically higher values (10%−40%) above 15 km than indicated by observations. The DOAS NO_2 observations on 9 October 2003 coincide with the model above 27 km and below 20 km within the given errors, but the model profile is up to 40% higher in-between. Model results for 24 March 2004 underestimate DOAS measurements below 20 km by 10%−20% and overestimate them above 22 km up to balloon float altitude by up to 20%.

Further photochemistry-related uncertainties in the SAOZ and DOAS observations are kept small when only using measurements for SZA≤88°, i.e. discarding solar occultation profiles from SAOZ and DOAS.

5 Results and discussion

Panels (a) and (b) in Figs. 3 to 7 show concentration and volume mixing ratio (VMR) profiles for the "best" backward match and panels (c) and (d) show corresponding profiles of the "best" forward match. Each panel shows the original measured, photochemically-uncorrected BrO balloon measurement (solid black squares) and the photochemically-corrected BrO profile (open blue squares), which is to be compared with the SCIAMACHY measurement of the corresponding "best" backward or forward match. The orbit number and time of each SCIAMACHY match are given in the label of each figure and in Table 1. Error bars of the photochemically-corrected profiles include the estimated error for the photochemical scaling as described in Sect. 2.3. Model profiles at the SZA of the balloon and the satellite observation are shown as solid and dashed green lines, respectively. Total inorganic Br_y volume mixing ratios as used in the model are also indicated as dash-dotted green line. The altitude range which fulfils the match criteria (as summarized in Table 1), is indicated by the thin dotted horizontal lines. In cases where only one horizontal line is plotted (e.g. backward match in Fig. 7), the match criteria are fulfilled above the indicated altitude, over the entire plotted range. SCIAMACHY measurements are shown as solid red circles in the matching altitude range and as open red circles outside. The SCIAMACHY error bars reflect precission and the vertical resolution is around 3 km. Certain orbits of Level 1 SCIAMACHY data remain unavailable and cannot be presented in this study. Total inorganic Br_y and its uncertainty, inferred from DOAS BrO as described above, is marked by dark blue vertical lines.

TRIPLE mid-latitude measurements on 24 September 2002 were performed between 55.6° and 67.9° SZA. The value SZA=60.1° was chosen as a scaling reference for the balloon observation. The SZA of the SCIAMACHY measurement is 45.1° for the backward match and 50.7° for the forward match. Since satellite and balloon measurements were taken in the morning well after sunrise, and the diurnal variation of BrO during the morning is rather small (see Fig. 2), the scaling over the entire altitude range is <5%, for both the backward and forward match. Model results over the entire altitude range are much larger than TRIPLE measurements. Comparing the dynamic tracers N_2O and CH_4 between model predictions and TRIPLE measurements, shows good agreement. NO_2 was scaled to match SCIAMACHY observations of the 10:32 UT limb scan of orbit 2968, the same forward match used for BrO comparison. SCIAMACHY NO_2 profiles tend to show lower values below 20 km than balloon validation measurements (Butz et al., 2005), possibly causing an overprediction of BrO in the model. However, even if no NO_2 scaling is performed in the model, modelled BrO is much higher than TRIPLE measurements. Thus, apart from unknown instrumental problems, the discrepancy between modelled and measured BrO cannot be explained. The time lag for the backward match between the satellite and the balloon measurement is quite short (−2.5 h) and match criteria are fulfilled between 16 and 33 km (see Table 1). For observations below 29 km the corresponding SCIAMACHY profile shows much large values and there is no agreement within the given error bars.

DOAS high-latitude ascent measurements taken on 23 March 2003 were performed between 77.9° and 88.8° SZA. For comparison the model output is plotted at 80.0° SZA. The photochemically corrected DOAS profile is obtained as described in Sect. 2.3 and by Butz et al. (2005). The SZAs of the SCIAMACHY backward and forward match are 81.2° and 57.7°, respectively. Compared to the TRIPLE flight, the scaling for the backward and forward match is higher (up to 15%) since DOAS measurements took place during late afternoon, before sunset. The agreement of the dynamic tracers N_2O and CH_4 between model predictions and LPMA measurements is warranted and NO_2 was scaled to DOAS measurements in the 1-D model, as described in Sect. 4. The overall agreement with the model is very convincing for the photochemically-uncorrected and corrected profiles. The SCIAMACHY profile for the backward (forward) match has a time delay of −5.2 (+17.4) h and match criteria are obeyed from 18 to 28 km (19 to 29 km). Below 25 km SCIAMACHY values for these profiles are in general higher than predicted but agree well within the error bars of the individual intruments.

DOAS mid-latitude ascent measurements taken on 9 October 2003 were performed between 71.0° and 81.5° SZA. For comparison purposes, the model output is plotted at 72.9° SZA. Since the SZAs of the SCIAMACHY backward and forward matches are 51.8° and 51.7°, respectively,

both scalings are similar. Due to strong oscillations of the gondola, measurements could only begin at ∼16 km, causing higher uncertainty of the lowest profile point at 18 km. Agreement of the dynamic tracers between model predictions and LPMA measurements could not be assessed, since no LPMA data is available to date. Therefore, dynamics were verified by O_3 measurements, which showed good agreement over the altitude range covered. NO_2 was scaled in the 1-D model as before. DOAS measurements coincide well with the model over the entire range. The backward (forward) match has a time delay of −6.5 (+17.2) h and match criteria obeyed above 17(25) km. SCIAMACHY values agree within the errors but again tend to show a high bias below 25 km.

SAOZ subtropical ascent measurements taken on 31 January 2004 before sunset were performed between 76° and 86° SZA and thus a scaling reference for the balloon observation of 80.2° SZA was used. The SZAs of the SCIAMACHY backward and forward match are both 36°. As for the DOAS flight, the scaling for the backward and forward match is significant. The agreement of the dynamics adopted in the model with observations could only be verified by comparing O_3 profiles also measured by the SAOZ instrument indicating that large dynamic uncertainties can be ruled out. Simultaneous measurements of NO_2 allowed it to be scaled in the 1-D model. Agreement with the model for BrO between 17 km and 25 km is convincing, but measurements below and above, are larger and even close to total Br_y. The comparison with a SCIAMACHY backward match shows agreement with the balloon measurements, although it is outside the matching altitude range. For the forward match a similar good agreement is found.

DOAS high-latitude ascent measurements taken on 24 March 2004 were performed between 74.6° and 85.4° SZA. For comparison the model output is plotted at 77.1° SZA. Since the SZAs of the SCIAMACHY backward and forward match are 68.3° and 61.8°, respectively, the scaling is very similar. Agreement of the dynamic tracers N_2O and CH_4 between model predictions and LPMA measurements could not be assessed, since no LPMA data is available to date. Therefore, dynamics could only be verified by O_3 measurements, which showed an overall good agreement over the entire altitude range. NO_2 was scaled in the 1-D model as before. The correspondence with the model is very convincing. The backward match has a time delay of −5.4 h and match criteria are obeyed between 12 and 33 km. The available SCIAMACHY profile for the forward match has a time delay of +17.1 h and match criteria are obeyed only between 20 and 26 km. As before the SCIAMACHY profiles show a high bias below 29 km but agree well within the errors.

Overall, the agreement of the balloon BrO observations from the 3 instruments with the model is encouraging. The tracer data measured by balloon instruments is found to correspond with the SLIMCAT CTM and therefore large uncertainties in vertical transport can be ruled out. All profiles fall within the constrained total Br_y and mostly agree with the

model within the error range. An exception is the TRIPLE flight, where the source of discrepancy is unclear, since dynamic and photochemical causes could be eliminated. After the scaling of NO$_2$ in the model, DOAS and SAOZ BrO profiles coincide with the model at almost every altitude within the errors (15 to 30% for DOAS and 25 to 50% for SAOZ, depending on altitude and measurement conditions).

For the SCIAMACHY retrievals presented here, it can be observed, that the Harvard-Smithsonian retrieval agrees within the given errors with the exception of the Triple comparison. However, the SCIAMACHY retrieval shows systematically higher values than expected from the photochemically-corrected balloon validation profiles and the model, for lower altitudes (below about 25 km). There is also an apparent change in the profile shape above about 25 km, which is especially obvious in the mixing ratio profiles. Here the SCIAMACHY values tend to decrease rapidly with increasing altitude and to be lower than predicted by the balloon measurements and the model. Disregarding the Triple comparsion, where there seems to be a systematic discrepency, the average agreement in the matching atlitude ranges, between the presented SCIAMACHY retrieval and the remote sensing balloon measurements (SAOZ and DOAS) above and below 25 km, is 20.5% and 19.8%, respectively.

Using the IUP-Bremen SCIAMACHY retrieval as described by Rozanov et al. (2005), the results presented by Rozanov et al. (2005) and Sinnhuber at al. (2005) and their conclusions, regarding SCIAMACHY BrO abundances, are different. The two comparisons with Triple BrO validation profiles (Rozanov et al., 2005) show lower values and better agreement, compared to the Harvard-Smithsonian retrieval presented here. As a result, Sinnhuber at al. (2005) using the results obtained with the IUP-Bremen retrieval (Rozanov et al., 2005), find SCIAMACHY BrO consistent with a photochemical model from 15 to 28 km when using a total Br$_y$ of 18 pptv. Similarly, Sioris et al. (2006) and Salawitch et al. (2005) find a better agreement with the Harvard-Smithsonian retrieval when increasing total Br$_y$ in their model to around 24 to 25 pptv. These discrepancies should encourage a further improvement of the different satellite retrievals.

Sources of error, which can influence the comparison between satellite and balloon measurements presented here, might be spatial variations of BrO within the match criteria of 1 h and 500 km, although this is very unlikely. Smaller discrepancies could be explained outside the matching altitude ranges, where air masses travelled along different trajectories that do not obey the match criteria. But overall the diurnal variation of BrO (without large spatial gradients) should be able to explain most of the scaling factor used to correct the profiles. The larger time delay for forward matches (see Table 1), and therefore the increasing uncertainty in the air mass trajectory calculation, could theoretically explain higher discrepancies compared to backward matches, but this is not the case for the present observations.

All balloon BrO validation flights, which are also listed in Table 1 but not presented in this study, were also photochemically-corrected to SCIAMACHY observations in order to obtain a set of corrected BrO profiles, which can be used for SCIAMACHY validation.

6   Conclusions

Stratospheric BrO abundances measured from 3 different balloon sensors were compared with reference to the 3-D CTM SLIMCAT model output. Model calculations were used to generate a BrO profile validation set for the new Envisat/SCIAMACHY satellite instrument and were compared with first retrieval exercises of SCIAMACHY BrO limb profiling. Since the diurnal variation of BrO and the spatial and temporal difference between the different observations prevent a direct comparison, the observations were considered with reference to outputs from the 3-D CTM. Air mass trajectory calculations were used to identify coincident SCIAMACHY limb measurements. The balloon-borne BrO profiles were photochemically scaled along the trajectories with a 1-D stratospheric chemistry model to match the photochemical conditions of the satellite observations. Model predictions were constrained by simultaneous observations with the balloon instruments, of dynamic and photochemical relevant parameters.

Total [Br$_y$]=(20.1±2.5) pptv obtained from DOAS BrO observations at mid-latitudes in 2003, served as an upper limit of the comparison. The good agreement of balloon trace gas measurements with the SLIMCAT model indicates that vertical transport is considered correctly and is not a major source of error. Within the given range of errors of the different measurement techniques, most of the balloon observations agree with model BrO. Initial BrO profiles available from the Harvard-Smithsonian SCIAMACHY retrieval agree on average to around 20% with the photochemically-corrected balloon observations (SAOZ and DOAS). An exception is the Triple profile, in which the balloon and satellite data mostly does not agree within the given errors. In general, the satellite measurements show systematically higher values below 25 km and a change in profile shape above about 25 km.

The presented set of BrO balloon profiles is meant to be representative and, according to the trajectory calculations, the most suitable set of SCIAMACHY BrO validation profiles and is thus recommended for future SCIAMACHY limb BrO retrieval exercises. The method and results discussed in this study are also of value for the validation of other existing satellite measurements of BrO (e.g. OMI (Levelt and Noordhoek, 2002)) or satellite instuments that intend to measure BrO in the future (e.g. GOME-2 (GOME-2 Products Guide , 2005)).

Digital copies of the BrO profiles for all validation flights can be obtained from the NILU data server (http://www.

nilu.no), upon signing the data protocol of the ESA sponsored Envisat validation activities. DOAS data is also available on http://www.iup.uni-heidelberg.de/institut/forschung/groups/atmosphere/stratosphere/.

References

Aliwell, S., Van Roozendael, M., Johnston, P., Richter, A., Wagner, T., Arlander, D., Burrows, J., Fish, D., Jones, R., Tornkvist, K., Lambert, J.-C., Pfeisticker, K., and Pundt, I.: Analysis for BrO in zenith-sky spectra: An intercomparison exercise for analysis improvement, J. Geophys. Res., 107, 2002.

Bösch, H., Camy-Peyret, C., Chipperfield, M., Fitzenberger, R., Harder, H., Schiller, C., Schneider, M., Trautmann, T., and Pfeilsticker, K.: Comparison of measured and modeled startospheric UV/visible actinic fluxes at large solar zenith angles, Geophys. Res. Lett., 28, 1179–1182, 2001.

Bösch, H., Camy-Peyret, C., Chipperfield, M. P., Fitzenberger, R., Harder, H., Platt, U., and Pfeilsticker, K.: Upper limits of stratospheric IO and OIO inferred from center-to-limb-darkening-corrected balloon-borne solar occultation visible spectra: Implications for total gaseous iodine and stratospheric ozone, J. Geophys. Res., 108, 4455, doi:10.1029/2002JD003078, 2003.

Bovensmann, H.: SCIAMACHY: Mission Objectives and Measurement Modes, J. Atmos. Sci., 56, 127–150, 1999.

Bracher, A., Sinnhuber, M., Rozanov, A., and Burrows, J. P.: Using a photochemical model for the validation of NO_2 satellite measurements at different solar zenith angles, Atmos. Chem. Phys., 5, 393–408, 2005, http://www.atmos-chem-phys.net/5/393/2005/.

Brune, W. H., Anderson, J. G., and Chan, K. R.: In situ observations of BrO over Antarctica: ER-2 aircraft results from 54° S to 72° S latitude, J. Geophys. Res., 94, 16 649–16 663, 1989.

Butz, A., Bösch, H., Camy-Peyret, C., Chipperfield, M., Dorf, M., Dufour, G., Grunow, K., Jeseck, P., Kühl, S., Payan, S., Pepin, I., Pukite, J., Rozanov, A., von Savigny, C., Sioris, C., Wagner, T., Weidner, F., and Pfeilsticker, K.: Inter-comparison of Stratospheric O_3 and NO_2 abundances retrieved from balloon borne direct sun observations and Envisat/SCIAMACHY limb measurements, Atmos. Chem. Phys., 5, 10 747–10 797, 2005.

Camy-Peyret, C., Flaud, J.-M., Perrin, A., Rinsland, C., Goldman, A., and Murcray, F.: Stratospheric N_2O_5, CH_4 and N_2O profiles from IR solar occultation spectra, J. Atmos. Chem., 16, 31–40, 1993.

Canty, T., Rivière, E., Salawitch, R., Berthet, G., Renard, J.-B., Pfeilsticker, K., Dorf, M., Butz, A., Bösch, H., Stimpfle, R., Wilmouth, D., Richard, E., Fahey, D., Popp, P., Schoeberl, M., Lait, L., and Bui, T.: Nighttime OClO in the winter Arctic vortex, J. Geophys. Res., 110, 1301, doi:10.1029/2004JD005035, 2005.

Chipperfield, M. P.: Multiannual simulations with a three-dimensional chemical transport model, J. Geophys. Res., 104, 1781–1805, 1999.

Chipperfield, M. P., Feng, W., and Rex, M.: Arctic ozone loss and climate sensitivity: Updated three-dimensional model study, Geophys. Res. Lett., 32, L11 813, doi:10.1029/2005GL022674, 2005.

Danilin, M. Y., Ko, M. K. W., Froidevaux, L., Santee, M. L., Lyjak, L. V., Bevilacqua, R. M., Zawodny, J. M., Sasano, Y., Irie, H., Kondo, Y., Russell, J. M., Scott, C. J., and Read, W. G.: Trajectory hunting as an effective technique to validate multiplatform measurements: Analysis of the MLS, HALOE, SAGE-II, ILAS, and POAM-II data in October–November 1996, J. Geophys. Res., 107(D20), 3–1, doi:10.1029/2001JD002012, 2002.

Deshler, T., Hervig, M., Hofmann, D., Rosen, J., and Liley, J.: Thirty years of in situ stratospheric aerosol size distribution measurements from Laramie, Wyoming (41° N), using balloon-borne instruments, J. Geophys. Res., 108, 4–1, doi:10.1029/2002JD002514, 2003.

Dufour, G., Payan, S., Lefevre, F., Berthet, G., Eremenko, M., Butz, A., Jeseck, P., Te, Y., Pfeilsticker, K., and Camy-Peyret, C.: 4-D comparison method to study NO_y partitioning in summer polar stratosphere. Influence of aerosol burden., Atmos. Chem. Phys., 5, 919–926, 2005, http://www.atmos-chem-phys.net/5/919/2005/.

Feng, W., Chipperfield, M., Davies, S., Sen, B., Toon, G., Blavier, J., Webster, C., Volk, C., Ulanovsky, A., Ravegnani, F., von der Gathen, P., Jost, H., Richard, E., and Claude, H.: Three-dimensional model study of the Arctic ozone loss in 2002/03 and comparison with 1999/2000 and 2003/04, Atmos. Chem. Phys., 5, 139–152, 2005, http://www.atmos-chem-phys.net/5/139/2005/.

Ferlemann, F., Camy-Peyret, C., Fitzenberger, R., Harder, H., Hawat, T., Osterkamp, H., Schneider, M., Perner, D., Platt, U., Vradelis, P., and Pfeilsticker, K.: Stratospheric BrO profiles measured at different latitudes and seasons: Instrument description, spectral analysis and profile retrieval, Geophys. Res. Lett., 25, 3847–3850, 1998.

Ferlemann, F., Bauer, N., Fitzenberger, R., Harder, H., Osterkamp, H., Perner, D., Platt, U., Scheider, M., Vradelis, P., and Pfeilsticker, K.: Differential optical absorption spectroscopy instrument for stratospheric balloon-borne trace gas studies, Appl. Opt., 39, 2377–2386, 2000.

Fish, D., Jones, R., and Strong, K.: Mid-latitude observations of the diurnal variation of stratospheric BrO, J. Geophys. Res., 100, 18 863–18 871, 1995.

EUMETSAT, GOME-2 Products Guide, available via http://www.eumetsat.int, EUM/OPS-EPS/MAN/05/0005, issue 1.0, 2005.

Harder, H., Camy-Peyret, C., Ferlemann, F., Fitzenberger, R., Hawat, T., Osterkamp, H., Schneider, M., Perner, D., Platt, U., Vradelis, P., and Pfeilsticker, K.: Stratospheric BrO profiles measured at different latitudes and seasons: atmospheric observations, Geophys. Res. Lett., 25, 3843–3846, 1998.

Harder, H., Bösch, H., Camy-Peyret, C., Chpperfield, M., Fitzenberger, R., Payan, S., Perner, D., Platt, U., Sinnhuber, B.-M., and Pfeilsticker, K.: Comparison of measured and modeled Stratospheric BrO: implications for the total amount of stratospheric bromine, Geophys. Res. Lett., 27, 3695–3698, 2000.

Hawat, T., Camy-Peyret, C., Jeseck, P., and Torguet, R.: Desciption and performance of a balloon-borne heliostat for solar absorption measurements, in: 12th ESA Symposium on Rocket and Balloon Programmes and Related Research, 1995.

Langematz, U., Labitzke, K., and Reimer, E.: Synoptic analysis and trajectories during the MAP/GLOBUS campaign 1983, Planet. Space Sci., 35, 525–538, 1987.

Lary, D. J.: Gas phase atmospheric bromine chemistry, J. Geophys. Res., 101, 1505–1516, 1996.

Lary, D. J. and Pyle, J. A.: Diffuse radiation, twilight and photochemistry, J. Atmos. Chem., 373–392, 1991.

Lary, D. J., Chipperfield, M. P., Toumi, R., and Lenton, T.: Heterogeneous atmospheric bromine chemistry, J. Geophys. Res., 101, 1489–1504, 1996.

Levelt, P. F. and Noordhoek, R.: OMI Algorithm Theoretical Basis Document Volume I: OMI Instrument, Level 0-1b Processor, Calibration & Operations, Tech. Rep. ATBD-OMI-01, Version 1.1, August 2002.

Lumpe, J. D., Fromm, M., Hopperl, K., Bevilacqua, R. M., Randall, C. E., Browell, E. V., Grant, W. B., McGee, T., Burris, J., Twigg, L., Richard, E. C., Toon, G. C., Margitan, J. J., Sen, B., Boesch, H., Fitzenberger, R., Pfeilsticker, K., Goutail, F., and Pommereau, J.-P.: Comparison of POAM III ozone measurements with correlative aircraft and balloon data during SOLVE, J. Geophys. Res., 107, 8316, doi:10.1029/2001JD000472, 2002.

McLinden, C. A., McConnell, J. C., Griffioen, E., and McElroy, C. T.: A vector radiative transfer model for the Odin/OSIRIS project, Can. J. Phys., 80, 375–393, 2002.

Montzka, S., Butler, J., Hall, B., Mondell, D., and Elkins, J.: A decline in tropospheric organic bromine, Geophys. Res. Lett., 30, 1826–1829, 2003.

Murphy, D. M., Thompson, D. S., and Middlebrock, A.: Bromine, iodine, and chlorine in single aerosol particles at Cap Grim, Geophys. Res. Lett., 24, 3197–3200, 1997.

Pfeilsticker, K., Sturges, W. T., Bösch, H., Camy-Peyret, C., Chipperfield, M. P., Engel, A., Fitzenberger, R., Müller, M., Payan, S., and Sinnhuber, B.-M.: Lower stratospheric organic and inorganic bromine budget for the Artic winter 1998/99, Geophys. Res. Lett., 27, 3305–3308, 2000.

Platt, U.: Differential optical absorption spectroscopy (DOAS), in: Air Monitoring by Spectroscopic Techniques, edited by: Sigrist, W. M., vol. 127, pp. 27–84, John Wiley & Sons, Inc., 1994.

Pundt, I., Pommereau, J.-P., Chipperfield, M., Roozendael, M. V., and Goutail, F.: Climatology of the stratospheric BrO vertical distribution by balloon-borne UV-visible spectrometry, J. Geophys. Res., 107, 23, doi:10.1029/2002JD002230, 2002.

Reimer, E. and Kaupp, H.: Source indentification of odour compounds using trajectories, Proc. ECO-INFORMA 97, Eco-Informa Press, Bayreuth, 572–577, 1997.

Rodgers, C.: Inverse methods for atmospheric sounding, World Scientific, Singapore, New Jersey, London, Hongkong, 2000.

Rozanov, A., Bovensmann, H., Bracher, A., Hrechanyy, S., Rozanov, V., Sinnhuber, M., Stroh, F., and Burrows, J. P.: NO_2 and BrO vertical profile retrieval from SCIAMACHY limb measurements: Sensitivity studies, Adv. Space Res., 36, 846–854, doi:10.1016/j.asr.2005.03.013, 2005.

Salawitch, R. J., Weisenstein, D. K., Kovalenko, L. J., Sioris, C. E., Wennberg, P. O., Chance, K., Ko, M. K. W., and McLinden, C. A.: Sensitivity of ozone to bromine in the lower stratosphere, Geophys. Res. Lett., 32, 5811, doi:10.1029/2004GL021504, 2005.

Sander, S., Friedl, R. R., Golden, D. M., Kurylo, M. J., Huie, R. E., Orkin, V. L., Ravishankara, A. R., Kolb, C. E., Molina, M. J., Moortgart, G. K., and Finlayson-Pitts, B. J.: Chemical kinetics and photochemical data for use in atmospheric studies, Technical Report, NASA/JPL Publication, 2003.

Schwab, J. J. and Anderson, J. G.: Oscillator Strengths of Cl(I) in the Vacuum Ultraviolet: The 2D–2P Transitions, J. Quant. Spectrosc. Radiat. Trans., 27, 445–457, 1987.

Sinnhuber, B. M., Rozanov, A., Sheode, N., Afe, O. T., Richter, A., Sinnhuber, M., Wittrock, F., Burrows, J. P., Stiller, G. P., von Clarmann, T., and Linden, A.: Global observations of stratospheric bromine monoxide from SCIAMACHY, J. Geophys. Res., 32, L20 810, doi:10.1029/2005GL023839, 2005.

Sioris, C., Haley, C., McLinden, C., von Savigny, C., McDade, I., McConnell, J., Evans, W., Lloyd, N., Chance, E. L. K., Kurosu, T., Murtagh, D., Frisk, U., Pfeilsticker, K., Bösch, H., Weidner, F., Strong, K., Stegman, J., and Megie, G.: Stratospheric profiles of nitrogen dioxide observed by OSIRIS on the Odin satellite, J. Geophys. Res., 108, 4215, doi:10.1029/2002JD002672, 2003.

Sioris, C. E., Kurosu, T., Martin, R., and Chance, K.: Stratospheric and tropospheric NO_2 observed by SCIAMACHY: first results, Adv. Space Res., 34, 780–785, 2004.

Sioris, C. E., Kovalenko, L. J., McLinden, C. A., Salawitch, R. J., Van Roozendael, M., Goutail, F., Dorf, M., Pfeilsticker, K., Chance, K., von Savigny, C., Liu, X., Kurosu, T. P., Pommereau, J. P., Bösch, H., and Frerick, J.: Latitudinal and vertical distribution of bromine monoxide in the lower stratosphere from SCIAMACHY limb scattering measurements, J. Geophys. Res., accepted, 2006.

Toohey, D. W., Anderson, J. G., Brune, W. H., and Chan, K. R.: In situ measurements of BrO in the Arctic stratosphere, Geophys. Res. Lett., 17, 513–516, 1990.

Van Roozendael, M. and Fayt, C.: WinDOAS 2.1. Software user manual, Belgium Institute for Space Aeronomie (BIRA/IASB), 2000.

Van Roozendael, M., Wagner, T., Richter, A., Pundt, I., Arlander, D., Burrows, J., Chipperfield, M., Fayt, C., Johnston, P., Lambert, J., Kreher, K., Pfeilsticker, K., Platt, U., Pommereau, J. P., Sinnhuber, B., Tornkvist, K., and Wittrock, F.: Intercomparison of BrO Measurements from ERS-2 GOME, Ground-based and balloon platforms, Adv. Space. Res., 29, 1161–1666, 2002.

Voigt, S., Orphal, J., Bogumil, K., and Burrows, J. P.: The tem-

perature dependence (203-293 K) of the absorption cross section of O_3 in the 230-850 nm region measured by Fourier-transform spectroscopy, J. Photochem. Photobiol. A, 143, 1–9, 2001.

Voigt, S., Orphal, J., and Burrows, J. P.: The Temperature- and Pressure-Dependence of the Absorption Cross-section of NO_2 in the 250–800 nm Region measured by Fourier-Transform Spectroscopy), J. Photochem. Photobiol A, 149, 1–7, 2002.

von der Gathen, P., Rex, M., Harris, N., Lucic, D., Knudsen, B., Braathen, G., Backer, H. D., Fabian, R., Fast, H., Gil, M., Kyr, E., Mikkelsen, I., Rummukainen, M., Sthelin, J., and Varotsos, C.: Observational evidence for chemical ozone depletion over the Arctic in winter 1991–92, Nature, 375, 131–134, 1995.

Wagner, T. and Platt, U.: Satellite mapping of enhanced BrO concentrations in the troposphere, Nature, 395, 486–490, 1998.

Wahner, A., Ravishankara, A., Sander, S., and Friedl, R.: Absorption cross section of BrO between 312 and 385 nm at 298 and 223 K, Chem. Phys. Lett., 152, 507–512, 1988.

Weidner, F., Bösch, H., Bovensmann, H., Burrows, J., Butz, A., Camy-Peyret, C., Dorf, M., Gerilowski, K., Gurlit, W., Platt, U., von Friedeburg, C., Wagner, T., and Pfeilsticker, K.: Balloon-borne limb profiling of UV/vis skylight radiances, O_3, NO_2, and BrO: technical set-up and validation of the method, Atmos. Chem. Phys., 5, 1409–1422, 2005, http://www.atmos-chem-phys.net/5/1409/2005/.

WMO: Scientific Assessment of Ozone depletion: 2002, World Meteorological Organization Global Ozone Research and Monitoring Project, Report 47, 2003.